A new R2 indicator for better hypervolume approximation

Ke Shang*
Shenzhen Key Laboratory of Computational Intelligence,
Department of Computer Science and Engineering,
Southern University of Science and Technology
Shenzhen, China
kshang@foxmail.com

Hisao Ishibuchi†
Shenzhen Key Laboratory of Computational Intelligence,
Department of Computer Science and Engineering,
Southern University of Science and Technology
Shenzhen, China
hisaoi@cs.osakafu-u.ac.jp

Min-Ling Zhang
School of Computer Science and Engineering,
Southeast University
Nanjing, China
zhangml@seu.edu.cn

Yiping Liu
Department of Computer Science and Intelligent Systems,
Osaka Prefecture University
Osaka, Japan
yiping0liu@gmail.com

ABSTRACT

In this paper, a new R2 indicator is proposed for better hypervolume approximation. First the fact that the original R2 indicator is not a good approximation for the hypervolume is illustrated by examples. Then the new R2 indicator is derived based on the Divergence theorem and Riemann sum approximation. The difference between the original R2 and the new R2 is only the added exponential in the new R2 where the exponential is the same as the dimensionality of the objective space (i.e., the number of objectives). The new R2, the original R2 and some other R2 variants are compared through comprehensive numerical studies on different solution sets under different scenarios. The results show the superiority of the proposed new R2 indicator over other R2 variants for the hypervolume approximation, where the new R2 indicator achieves the best linear relation with the true hypervolume.

CCS CONCEPTS

• **Mathematics of computing → Mathematical optimization**;

KEYWORDS

Hypervolume approximation, R2 indicator, Divergence theorem, Riemann sum

ACM Reference Format:
Ke Shang, Hisao Ishibuchi, Min-Ling Zhang, and Yiping Liu. 2018. A new R2 indicator for better hypervolume approximation. In *GECCO '18: Genetic and Evolutionary Computation Conference, July 15–19, 2018, Kyoto, Japan.* ACM, New York, NY, USA, 8 pages. https://doi.org/10.1145/3205455.3205543

*Also with Southeast University.
†Also with Osaka Prefecture Univeristy.

GECCO '18, July 15–19, 2018, Kyoto, Japan

ACM ISBN 978-1-4503-5618-3/18/07…$15.00
https://doi.org/10.1145/3205455.3205543

1 INTRODUCTION

Hypervolume [20] is a widely used performance indicator in the Evolutionary Multi-objective Optimization (EMO) community. It is not only widely used for the performance evaluations of the Evolutionary Multi-objective Optimization Algorithms (EMOA) but also adopted as a key component in the indicator-based EMOAs (e.g., SMS-EMOA [3], HypE [2]) due to its well-known unique property (i.e., Pareto compliance) among all the existing indicators. The bottleneck of the hypervolume application in EMOA is the increasing computational burden as the dimentionality of the objective space increases. Efforts in the hypervolume approximation [2, 8] have been done to increase the applicability of the hypervolume to high-dimensional spaces.

Currently there are mainly two methods to approximate the hypervolume. The first method is based on the monte carlo hit-or-miss method [1, 2]. A large number of points are evenly sampled in a predefined sampling space which is a subspace of the objective space. A point is called a hit if it is included in the hypervolume set, otherwise it is called a miss. Then the hypervolume is approximated by the ratio of the number of hits to the total number of the sampled points multiplies the volume of the sampling space. The second method is based on the achievement scalarizing functions [8, 9]. The hypervolume is approximated by a number of achievement scalarizing functions with uniformly distributed weight vectors. Each achievement scalarizing function with a different weight vector is used to measure the distance from the reference point to the hypervolume attainment surface. Then the average distance from the reference point to the attainment surface over a large number of weight vectors is calculated as the hypervolume approximation.

The R2 indicator is another popular performance indicator in the EMO field. It was initially introduced in [7] and later has been further investigated in [4, 13, 19]. The R2 indicator is based on utility functions, and most studies [4, 6, 14, 17] of the R2 indicator are based on the standard weighted Tchebycheff function. Later on in [13], a modified R2 indicator is proposed based on a new Tchebycheff function which is called 2-Tch. The modified R2 indicator shows a clearer geometric property to approximate the hypervolume. To be more specific, the modified R2 indicator can be

indirectly used as the second method mentioned above for the hypervolume approximation. The second method that uses different line segments starting from the reference point to the attainment surface of the solution sets for the hypervolume approximation can be formularized in the form of the R2 indicator.

In this paper, we further investigate the hypervolume approximation method by the R2 indicator. By using two simple toy examples, we point out that the original R2 indicator is actually not a good approximation for the hypervolume because the relation between the R2 indicator and the true hypervolume is not linear. Motivated by the volume estimation method for high-dimensional polytopes in [10], a formula for hypervolume approximation is derived based on the Divergence theorem and Riemann sum approximation. Then a new R2 indicator is extracted from this formula. Interestingly, the new R2 indicator and the original R2 indicator are very similar except that there is an extra exponential in the new R2 indicator. This small change in the R2 indicator significantly improves the approximation quality for the hypervolume. In order to verify the effectiveness of the proposed new R2 indicator for the hypervolume approximation, comprehensive numerical studies are conducted on different solution sets under different scenarios. The results show that the new R2 indicator achieves the best linear relation with the hypervolume among several different R2 variants including the original R2 indicator and some other R2 indicators which are proposed for comparison.

The remainder of the paper is organized as follows. Section 2 gives the preliminaries of the paper. A new R2 indicator is proposed for better hypervolume approximation in Section 3. Numerical studies are given in Section 4 to test the effectiveness of the proposed new R2. Lastly we conclude the paper in Section 5.

2 PRELIMINARIES

2.1 Hypervolume

Given a reference point $\mathbf{r}$ and an approximation solution set A, the hypervolume of the set A is defined as:

$$HV(A,\mathbf{r}) = \mathcal{L}\left(\bigcup_{\mathbf{a}\in A}\{\mathbf{b}|\mathbf{a}\succ\mathbf{b}\succ\mathbf{r}\}\right). \tag{1}$$

where $\mathcal{L}(.)$ is the Lebesgue measure of a set, and $\mathbf{a}\succ\mathbf{b}$ means $\mathbf{a}$ dominates $\mathbf{b}$.

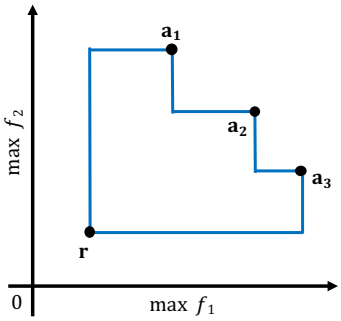

Figure 1: An illustration of the hypervolume.

Fig. 1 gives an illustration of the hypervolume in a two-dimension objective space with three solutions. The hypervolume is the area of the enclosed polygon by the blue lines.

2.2 R2 indicator

Given a solution set A, a set of weight vectors W, and a utopian point $\mathbf{r}^*$, the R2 indicator based on the standard weighted Tchebycheff function is defined as:

$$R_2^{te}(A,W,\mathbf{r}^*) = \frac{1}{|W|}\sum_{\mathbf{w}\in W}\min_{\mathbf{a}\in A}\left\{g^{te}(\mathbf{a}|\mathbf{w},\mathbf{r}^*)\right\} \tag{2}$$

where the standard weighted Tchebycheff function is defined as:

$$g^{te}(\mathbf{a}|\mathbf{w},\mathbf{r}^*) = \max_{j\in\{1,\ldots,m\}}\left\{w_j|r_j^* - a_j|\right\} \tag{3}$$

where $\mathbf{w} = (w_1, w_2, \ldots, w_m)$ is a given weight vector with $\|\mathbf{w}\|_1 = 1$ and $w_1, w_2, \ldots, w_m \geq 0$.

In [13], a modified R2 indicator is proposed based on a new Tchebycheff function. The modified R2 indicator shows a clearer geometric property to approximate the hypervolume.

Given a solution set A, a set of direction vectors Λ, and a utopian point $\mathbf{r}^*$, the modified R2 indicator based on the 2-Tch function is defined as:

$$R_2^{2tch}(A,\Lambda,\mathbf{r}^*) = \frac{1}{|\Lambda|}\sum_{\lambda\in\Lambda}\min_{\mathbf{a}\in A}\left\{g^{2tch}(\mathbf{a}|\lambda,\mathbf{r}^*)\right\} \tag{4}$$

where the 2-Tch function is defined as:

$$g^{2tch}(\mathbf{a}|\lambda,\mathbf{r}^*) = \max_{j\in\{1,\ldots,m\}}\left\{\frac{|r_j^* - a_j|}{\lambda_j}\right\} \tag{5}$$

where $\lambda = (\lambda_1, \lambda_2, \ldots, \lambda_m)$ is a given direction vector with $\|\lambda\|_2 = 1$ and $\lambda_1, \lambda_2, \ldots, \lambda_m \geq 0$.

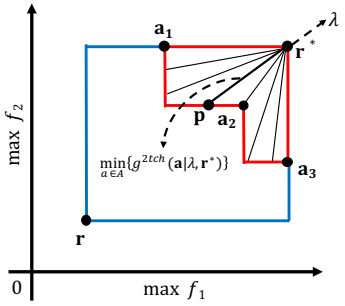

Figure 2: An illustration of the geometric property of R_2^{2tch}.

Fig. 2 shows an illustration of the geometric property of R_2^{2tch} in a two-dimensional objective space with three solutions. In this figure, $\mathbf{r}^*$ is the utopian point and $\mathbf{r}$ is the reference point for hypervolume calculation. Given a direction vector λ, suppose that a line follows the direction λ and passes through $\mathbf{r}^*$, $\mathbf{p}$ is the intersection point of this line and the attainment surface of the solution set, then the length of the line segment with the end points $\mathbf{r}^*$ and $\mathbf{p}$ is just the value of $\min_{\mathbf{a}\in A}\left\{g^{2tch}(\mathbf{a}|\lambda,\mathbf{r}^*)\right\}$, and the value of R_2^{2tch} is the average length of the line segments with different directions as shown in Fig. 2.

2.3 R2 for hypervolume approximation

The idea of using different line segments starting from a reference point to the attainment surface of the solution sets for the hypervolume approximation is firstly proposed in [8]. Intuitively, the average length of the line segments in Fig. 3 is closely related to the hypervolume.

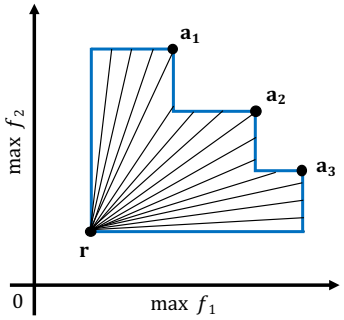

Figure 3: An illustration of the hypervolume approximation.

The R_2^{2tch} indicator cannot be directly used for the hypervolume approximation as shown in Fig. 2. In order to allow the R_2^{2tch} indicator to be able to directly approximate the hypervolume, its modified version is defined as:

$$R_2^{mtch}(A,\Lambda,\mathbf{r}) = \frac{1}{|\Lambda|}\sum_{\lambda\in\Lambda}\max_{\mathbf{a}\in A}\left\{g^{mtch}(\mathbf{a}|\lambda,\mathbf{r})\right\} \tag{6}$$

where g^{mtch} function is defined as:

$$g^{mtch}(\mathbf{a}|\lambda,\mathbf{r}) = \min_{j\in\{1,\ldots,m\}}\left\{\frac{|r_j - a_j|}{\lambda_j}\right\} \tag{7}$$

where $\mathbf{r}$ is the reference point for the hypervolume calculation, λ is a given direction vector which is the same as in g^{2tch} in Eq. (5).

Now the R_2^{mtch} indicator has a geometric property as shown in Fig. 3, which can be used directly for the hypervolume approximation.

3 NEW R2 INDICATOR

3.1 Examination of R_2^{mtch} indicator

A simple example is given to illustrate that the R_2^{mtch} indicator is actually not a good approximation for the hypervolume.

Example 3.1. Consider a 1/4 circle in the first quadrant with the radius r and the center at the origin. Suppose that the reference point is the origin and the 1/4 circle is the solution set of a two-objective maximization problem. Then the hypervolume of the solution set is the area of the 1/4 circle which is $\pi r^2/4$, while R_2^{mtch} is the average length of the line segments starting from the origin to the 1/4 circle which is a constant r. We can see that the relation between the hypervolume and R_2^{mtch} is not linear with respect to r. In this case, the R_2^{mtch} indicator is not a good approximation for the hypervolume.

Let us consider another two-objective example with a linear Pareto front $f_1 + f_2 = 1$ and $f_1, f_2 \geq 0$.

Example 3.2. An initial solution set A_1 is generated as $A_1 = \{(0,1),(1/H,1-1/H),(2/H,1-2/H),\ldots,(1,0)\}$ where $H = 100$, then 100 solution sets are generated as $A_i = \{(0,i),(i/H,i-i/H),(2i/H,i-2i/H),\ldots,(i,0)\}$ where $i = 1,2,\ldots,100$. Each solution set has $H+1$ solutions. All solutions in the i-th solution sets are on the line $f_1 + f_2 = i$. The hypervolume and R_2^{mtch} indicator are calculated for each solution set where 10000 direction vectors[1] are used in R_2^{mtch} and the results are shown in Fig. 4. Fig. 4 (a) and (b) show the hypervolume and the R_2^{mtch} results respectively[2]. The relation between the hypervolume and R_2^{mtch} is shown in Fig. 4 (c) where we can observe a clear nonlinear relation. This observation indicates that the R_2^{mtch} indicator is indeed not a good approximation for the hypervolume.

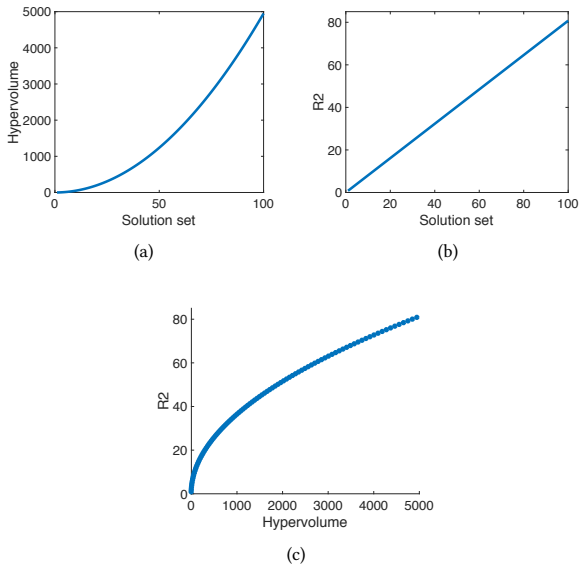

Figure 4: Numerical results of Example 3.2.

3.2 Proposal of a new R2 indicator

In [10], the volume of a high-dimensional polytope is calculated by using Gauss's divergence theorem. Borrowing the idea in [10], the hypervolume can be calculated by means of volume integral and surface integral.

In Section 2.1, the hypervolume is defined upon a set $V = \bigcup_{\mathbf{a}\in A}\{\mathbf{b}|\mathbf{a} \succ \mathbf{b} \succ \mathbf{r}\}$, and $V \subset \mathbb{R}^m$ is compact and has a piecewise smooth boundary. If $\mathbf{F}$ is a continuously differentiable vector field defined on a neighborhood of V and its divergence is constant $\nabla \cdot \mathbf{F} = 1$, then we have:

$$HV(V) = \iiint_V dV = \iiint_V (\nabla\cdot\mathbf{F})dV = \oiint_S (\mathbf{F}\cdot\mathbf{n})dS. \tag{8}$$

[1]The direction vectors are generated as follows: First use the simplex lattice design method [18] to generate a set of weight vectors, then for each weight vector $\mathbf{w}$, the corresponding direction vector $\lambda = \mathbf{w}/\|\mathbf{w}\|_2$.

[2]For convenience, we will use "R2" to represent the R_2^{mtch} indicator in the figures and tables of the paper.

where dV is the volume element on V, S is the boundary of V and dS is the $(m-1)$-dimensional volume element on S, $\mathbf{n}$ is the outer normal vector on the boundary.

If the vector field $\mathbf{F}(\mathbf{f}) = \frac{1}{m}\mathbf{f}$, then its divergence $\nabla \cdot \mathbf{F} = 1$. Fig. 5 shows the vector filed $\mathbf{F}(\mathbf{f}) = \frac{1}{2}\mathbf{f}$ in a two-dimensional space.

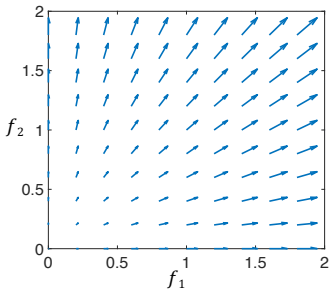

Figure 5: Vector field $\mathbf{F}(\mathbf{f}) = \frac{1}{2}\mathbf{f} = \frac{1}{2}(f_1, f_2)$.

Substituting $\mathbf{F}$ with $\frac{1}{m}\mathbf{f}$ in Eq. (8), we have:

$$\oiint_S (\mathbf{F}\cdot\mathbf{n})dS = \oiint_S (\frac{1}{m}\mathbf{f}\cdot\mathbf{n})dS = \frac{1}{m}\oiint_S (\mathbf{f}\cdot\mathbf{n})dS. \quad (9)$$

Now the hypervolume is transformed into a surface integral as shown in Eq. (9). For convenience, the hypervolume domain is shifted and reflected in order to let the reference point $\mathbf{r}$ lying on the origin and the hypervolume domain contained in the first quadrant.

Fig. 6 gives an illustration of how to calculate the surface integral. In Fig. 6, the boundaries of the hypervolume domain are depicted by the blue and red lines. For a point $\mathbf{f}$ on the boundary as shown in this figure, we know that $\|\mathbf{f}\|_2 = \max_{\mathbf{a}\in A}\left\{g^{mtch}(\mathbf{a}|\lambda,\mathbf{r})\right\}$ where λ is the direction vector. So we have $\mathbf{f} = \|\mathbf{f}\|_2\,\lambda$. The normal vector $\mathbf{n}$ is also shown for the corresponding $\mathbf{f}$. Let $\mathbf{a}^* = \arg\max_{\mathbf{a}\in A}\left\{g^{mtch}(\mathbf{a}|\lambda,\mathbf{r})\right\}$, then the normal vector $\mathbf{n} = (\mathbf{f} == \mathbf{a}^*)$[3]. Notice that on the blue boundaries (i.e., line segments **op** and **oq**), $\mathbf{f}\cdot\mathbf{n} = 0$ because the two vectors $\mathbf{f}$ and $\mathbf{n}$ are orthogonal. So only the red boundaries are useful for calculating the integral, and the red boundaries exactly constitute the hypervolume attainment surface.

In practice, it is very difficult to calculate the integral in Eq. (9) directly even if $\mathbf{f}$ and $\mathbf{n}$ can be calculated. One way is to use the Riemann sum to approximate the integral as follows:

$$\frac{1}{m}\oiint_S (\mathbf{f}\cdot\mathbf{n})dS = \frac{1}{m}\oiint_{S'} (\mathbf{f}\cdot\mathbf{n})dS' \approx \frac{1}{m}\sum_{i=1}^{N}(\mathbf{f}_i\cdot\mathbf{n}_i)\Delta S_i. \quad (10)$$

where S' is the hypervolume attainment surface and $S' = \bigcup_{i=1}^{N} S_i$, $\mathbf{f}_i \in S_i$, $\mathbf{n}_i$ is the normal vector at point $\mathbf{f}_i$, ΔS_i is the $(m-1)$-dimensional volume of S_i.

Now an approximation for ΔS_i is needed. Using the idea in [10], the volume element on the unit sphere is utilized for this approximation. The surface area of the unit m-sphere is $S_{sphere} = 2\pi^{m/2}/\Gamma(m/2)$ where Γ is the gamma function. Uniformly dividing the unit m-sphere in the first quadrant into N parts, the surface area of each part is $\Delta S_{sphere} = S_{sphere}/(2^m N)$, then ΔS_i is approximated by the projection of ΔS_{sphere} to the boundary at $\mathbf{f}_i$ by a factor of $\|\mathbf{f}_i\|_2^{m-1}/(\lambda_i\cdot\mathbf{n}_i)$. Then we have:

$$\begin{aligned} HV(V) &\approx \frac{1}{m}\sum_{i=1}^{N}(\mathbf{f}_i\cdot\mathbf{n}_i)\Delta S_i \\ &\approx \frac{1}{m}\sum_{i=1}^{N}(\mathbf{f}_i\cdot\mathbf{n}_i)\Delta S_{sphere}\,\|\mathbf{f}_i\|_2^{m-1}/(\lambda_i\cdot\mathbf{n}_i) \\ &= \frac{1}{m}\sum_{i=1}^{N}\Delta S_{sphere}\,\|\mathbf{f}_i\|_2^{m} \\ &= \frac{\pi^{m/2}}{mN2^{m-1}\Gamma(m/2)}\sum_{i=1}^{N}\|\mathbf{f}_i\|_2^{m} \\ &= \frac{\pi^{m/2}}{m|\Lambda|2^{m-1}\Gamma(m/2)}\sum_{\lambda\in\Lambda}\max_{\mathbf{a}\in A}\left\{g^{mtch}(\mathbf{a}|\lambda,\mathbf{r})\right\}^m. \end{aligned} \quad (11)$$

where Λ is the set of the direction vectors corresponding to $\mathbf{f}_i, i = 1,\ldots,N$.

Now an approximation for the hypervolume is obtained. Notice that in Eq. (11), the parameters $\pi^{m/2}$, m, 2^{m-1} and $\Gamma(m/2)$ are all constants in an m-dimensional space. Based on this observation, we only extract the useful components from Eq. (11) to formulate a new R2 indicator as follows:

$$R_2^{new}(A,\Lambda,\mathbf{r}) = \frac{1}{|\Lambda|}\sum_{\lambda\in\Lambda}\max_{\mathbf{a}\in A}\left\{g^{mtch}(\mathbf{a}|\lambda,\mathbf{r})\right\}^m. \quad (12)$$

Comparing Eq. (12) with Eq. (6), we can see that the only difference between R_2^{mtch} and R_2^{new} is the added exponential m in R_2^{new}.

Let us revisit the two examples in Section 3.1. In Example 3.1, the R_2^{new} indicator is r^2, then the relation between the hypervolume and R_2^{new} is linear with respect to r. In Example 3.2, the same solution sets as in Fig. 4 are used for calculating R_2^{new}. The results are shown in Fig. 7[4]. In Fig. 7 (c), we can observe a clear linear relation between the hypervolume and the R_2^{new}, which shows that the R_2^{new} indicator is a good approximation for the hypervolume.

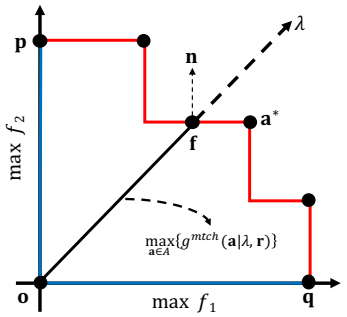

Figure 6: Illustration of the calculation of the surface integral in Eq. (9).

[3] $\mathbf{f} == \mathbf{a}^*$ is an element-wise logical operation, where a 0-1 vector is returned with 1 element if the two compared elements are equal and 0 element otherwise.

[4] For convenience, we will use "New R2" to represent the R_2^{new} indicator in the figures and tables of the paper.

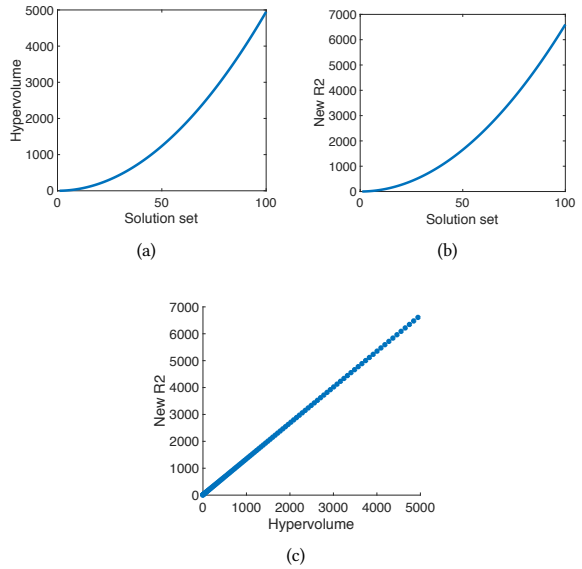

Figure 7: Numerical results of Example 3.2.

The above-mentioned experimental results on the two toy examples suggest that the R_2^{new} indicator is better than the R_2^{mtch} indicator for the hypervolume approximation. In the next section, comprehensive numerical studies are conducted on different solution sets under different scenarios to test the effectiveness of the R_2^{new} indicator for the hypervolume approximation.

4 NUMERICAL STUDIES

4.1 Scenario 1: Regular solution sets with different number of objectives

First we examine the solution sets on the linear Pareto front $f_1 + f_2 + ... + f_m = 1$ and $f_1, f_2, ..., f_m \geq 0$ for $m = 3, 4, 5$.

An initial solution set A_1^m is generated by the simplex lattice design method [18] for each m. The solution number #S in the initial solution set A_1^m is shown in the second column of Table 1. Then a predefined number of solution sets are generated as A_i^m where $i = 1, 2, ..., \#SS$ and #SS is the number of solution sets as shown in the third column of Table 1. For each solution $(f_1, f_2, ..., f_m)$ in the initial solution set A_1^m, the corresponding solution in A_i^m is generated as $(i \cdot f_1, i \cdot f_2, ..., i \cdot f_m)$. The hypervolume, R_2^{mtch} and R_2^{new} are calculated for each solution set. A predefined number #DV of direction vectors in the fourth column of Table 1 are used in R_2^{mtch} and R_2^{new}. The reference point $\mathbf{r}$ is set as the origin.

The results are shown in Fig. 8. The left column figures show the relation between the hypervolume and R_2^{mtch} and the right column figures show the relation between the hypervolume and R_2^{new}. We can observe a clear nonlinear relation between the hypervolume and R_2^{mtch} and a clear linear relation between the hypervolume and R_2^{new}, which suggests that R_2^{mtch} is not a good approximation for the hypervolume while R_2^{new} can approximate the hypervolume very well.

Table 1: Parameter settings in Section 4.1

m	#S[1]	#SS[2]	#DV[3]
3	91	100	9870
4	56	50	9880
5	40	30	8855

[1] The number of solutions in each solution set.
[2] The number of solution sets.
[3] The number of direction vectors.

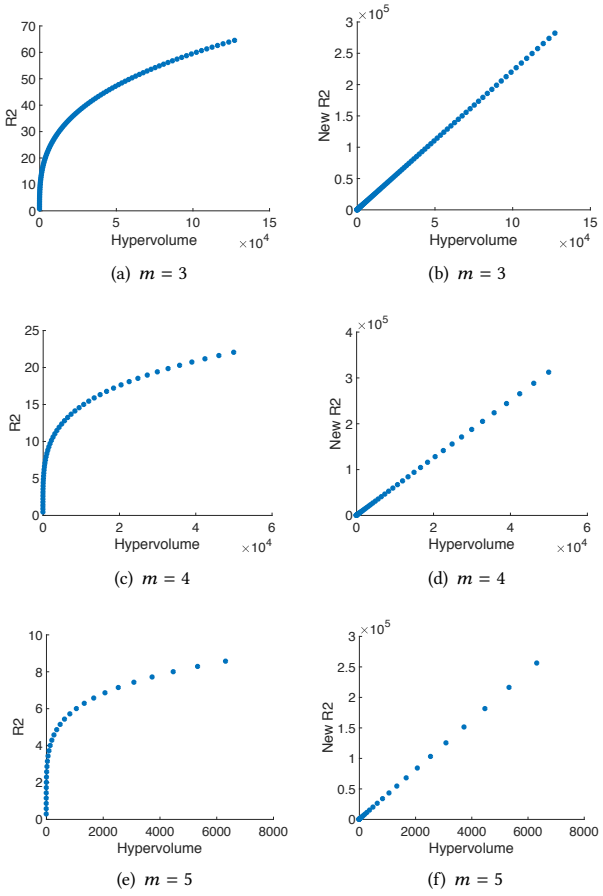

Figure 8: Numerical results in Section 4.1

Let us recall that the only difference between R_2^{mtch} and R_2^{new} is the added exponential m in R_2^{new}. It seems that the exponential m plays an important role for improving the approximation ability from R_2^{mtch} to R_2^{new}. So, it would be interesting to examine the effect of the exponential part by changing its value on the approximation ability of the R2 indicator through computational experiments. More specifically, we examine the approximation ability of the following variant of the R2 indicator:

$$R_2^{compare}(A, \Lambda, \mathbf{r}) = \frac{1}{|\Lambda|} \sum_{\lambda \in \Lambda} \max_{\mathbf{a} \in A} \left\{ g^{mtch}(\mathbf{a}|\lambda, \mathbf{r}) \right\}^{m'}. \quad (13)$$

where m' is an arbitrary integer which is different from m.

We calculate the $R_2^{compare}$ indicator on the solution sets $A_i^5, i = 1, 2, ..., 30$. In this case (i.e., $m = 5$), we choose $m' = 2, 3, 4, 6, 7, 8$. The number of direction vectors used in $R_2^{compare}$ is the same as in R_2^{mtch} and R_2^{new}. The comparison results among R_2^{mtch}, R_2^{new} and $R_2^{compare}$ are shown in Fig. 9[5]. All the values are normalized in order to have a clear visual comparison.

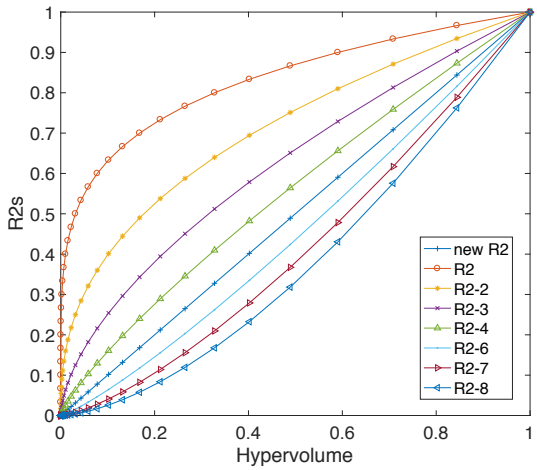

Figure 9: Comparison results among different R2 indicators.

From Fig. 9, we can see that the R_2^{new} indicator achieves the best approximation ability among all the R2 variants, which has a linear relation with the hypervolume. We can also observe that the relation between the hypervolume and the R2 indicators tends to become more linear with the increase of the parameter m' from 1 to 5 and achieves the best linearity when $m' = 5$, then the relation becomes nonlinear again with the continued increase of m' from 5 to 8. From this observartion we can see that the exponential m in R_2^{new} plays a key role for achieving a good approximation for the hypervolume. A larger or smaller exponential than m will worsen the approximation performance of the R2 indicator.

4.2 Scenario 2: Regular solution sets with random reference points

Now we examine the solution sets on a linear triangular Pareto front and linear inverted triangular Pareto front in a three-dimensional objective space for different specification of a reference point.

The solution set on the linear triangular Pareto front is the same as the solution set A_1^3 generated in Section 4.1. The solution set on the linear inverted triangular Pareto front B_1^3 is generated from A_1^3 as follows: for each solution $(f_1, f_2, f_3) \in A_1^3$, the corresponding solution in B_1^3 is generated as $(1-f_1, 1-f_2, 1-f_3)$. Then 100 reference points $\mathbf{r}_i, i = 1, 2, ..., 100$ are randomly sampled in the cube $[-1, 0] \times [-1, 0] \times [-1, 0]$. Denoting the corresponding solution sets of A_1^3 and B_1^3 with reference point $\mathbf{r}_i$ as A_i^3 and B_i^3 respectively, then we obtain 200 solution sets A_i^3 and B_i^3, $i = 1, ..., 100$. The hypervolume, R_2^{mtch}, R_2^{new} and $R_2^{compare}(m' = 2, 4, 5)$ are calculated for each solution set. The number of the direction vectors for the R2 calculation is the same as in Table 1.

Fig. 10 shows the comparison results among different R2 indicators. All the values are normalized. Fig. 10 (a) and (b) are the results for solution sets A_i^3 and B_i^3 respectively. In Fig. 10 we can see that the R_2^{new} indicator achieves the best approximation performance among all the R2 indicators which has the best linearity relation. But the visual difference among different R2 indicators is not so obvious since some other R2 indicators also seem to have a good linear relation with the hypervolume. In order to precisely compare the approximation quality of the R2 indicators, we use the following two metrics $\rho(\mathbf{x}, \mathbf{y})$ and $L(\mathbf{x}, \mathbf{y})$:

$$\rho(\mathbf{x}, \mathbf{y}) = \frac{\text{cov}(\mathbf{x}, \mathbf{y})}{\sigma_{\mathbf{x}} \sigma_{\mathbf{y}}}. \tag{14}$$

where $\text{cov}(\mathbf{x}, \mathbf{y})$ is the covariance of $\mathbf{x}$ and $\mathbf{y}$, $\sigma_{\mathbf{x}}$ and $\sigma_{\mathbf{y}}$ are the standard deviations of $\mathbf{x}$ and $\mathbf{y}$ respectively.

$$L(\mathbf{x}, \mathbf{y}) = \frac{1}{N} \|\mathbf{x} - \mathbf{y}\|_2^2. \tag{15}$$

where N is the dimensionality of $\mathbf{x}$ and $\mathbf{y}$.

Eq. (14) is the Pearson correlation coefficient which is a measure of the linear correlation between $\mathbf{x}$ and $\mathbf{y}$, where 1 is the total positive linear correlation, 0 is no linear correlation, and -1 is the total negative linear correlation. It is used to evaluate the approximation quality of the R2 indicators on the defined solution sets. Eq. (15) is the Mean Squared Error (MSE) between $\mathbf{x}$ and $\mathbf{y}$. For the normalized hypervolume and the R2 indicators, the ideal linear relation is the line $y = x$ where y represents the hypervolume and x represents the R2 indicators. So the MSE can be used to evaluate how far the R2 indicators are from the ideal linear relation for the hypervolume approximation.

First we calculate the Pearson correlation coefficients between the hypervolume and the R2 indicators. The results are given in Table 2. Table 2 clearly shows that the R_2^{new} indicator has the highest correlation coefficient, which means that the R_2^{new} indicator achieves the best linear relation among all the R2 indicators. Then we calculate the MSE between the hypervolume and the R2 indicators. The results are given in Table 3. The R_2^{new} has the smallest MSE value compared to other R2 indicators, which means that R_2^{new} is the closest to the ideal linear relation. The results of the two metrics clearly show the superiority of the R_2^{new} indicator over other R2 indicators for the hypervolume approximation.

Table 2: Correlation coefficients between hypervolume and R2 indicators in Section 4.2

Indicators	Triangular Pareto front	Inverted triangular Pareto front
R2	0.9845	0.9933
New R2	**0.9998**	**0.9990**
R2-2	0.9956	0.9981
R2-4	0.9979	0.9967
R2-5	0.9912	0.9918

[5]For convenience, we will use "R2-m'" to represent the $R_2^{compare}$ indicator in the figures and tables of the paper.

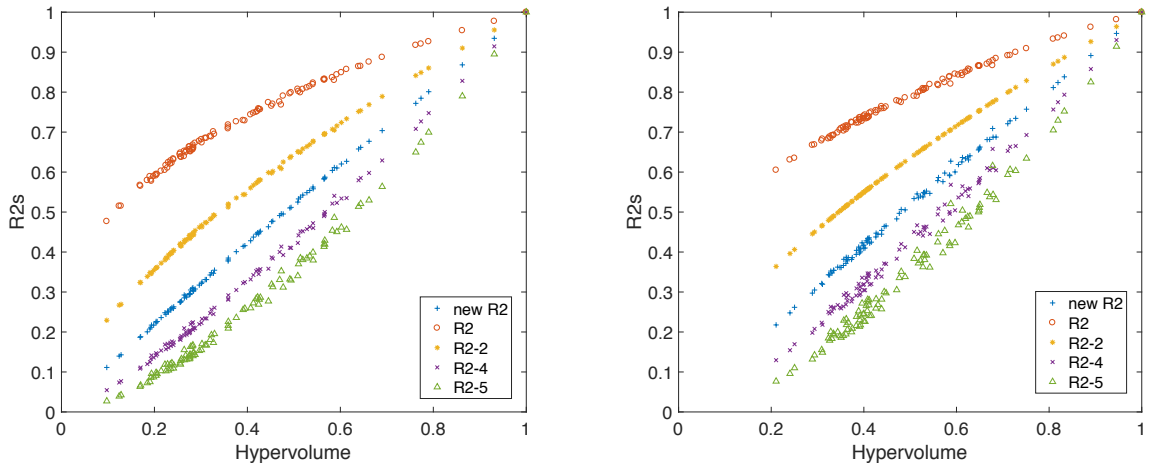

(a) Triangular Pareto front

(b) Inverted triangular Pareto front

Figure 10: Numerical results in Section 4.2.

Table 3: MSE between hypervolume and R2 indicators in Section 4.2

Indicators	Triangular Pareto front	Inverted triangular Pareto front
R2	1.1414e-01	8.8036e-02
New R2	**4.1379e-04**	**2.6180e-04**
R2-2	2.1586e-02	1.7763e-02
R2-4	4.5632e-03	5.6370e-03
R2-5	1.6927e-02	2.0541e-02

4.3 Scenario 3: Random solution sets with different number of solutions

In this section, we examine the solution sets of different size on a linear triangular Pareto front and linear inverted triangular Pareto front in a three-dimensional objective space. The linear triangular Pareto front is $f_1 + f_2 + f_3 = 1$ and $f_1, f_2, f_3 \geq 0$ and the linear inverted triangular Pareto front is $f_1+f_2+f_3 = 2$ and $0 \leq f_1, f_2, f_3 \leq 1$.

Solution sets on the linear triangular Pareto front and linear inverted triangular Pareto front are generated by sampling i points on the corresponding Pareto fronts where $i = 1, \ldots, 100$. A total number of 200 solution sets are obtained. The hypervolume, R_2^{mtch}, R_2^{new} and $R_2^{compare}(m' = 2, 4, 5)$ are calculated for each solution set. The number of direction vectors for R2 calculation is the same as in Table 1. The reference point $\mathbf{r}$ is set as the origin.

Fig. 11 shows the comparison results among different R2 indicators. All the values are normalized. Fig. 11 (a) is the results on the solution sets with the linear triangular Pareto front and Fig. 11 (b) is the results on the solution sets with the linear inverted triangular Pareto front. It seems that the R_2^{new} indicator has the best linear relation in Fig. 11. Table 4 shows the correlation coefficients between the hypervolume and the R2 indicators. It is clear in Table 4 that the R_2^{new} indicator has the highest correlation coefficient among all the R2 indicators. Table 5 gives the MSE between the hypervolume and the R2 indicators. From Table 5 we can see that R_2^{new} has the smallest MSE value compared to other R2 indicators. The results of the two metrics clearly show the superiority of the R_2^{new} indicator over other R2 indicators for the hypervolume approximation.

Table 4: Correlation coefficients between hypervolume and R2 indicators in Section 4.3

Indicators	Triangular Pareto front	Inverted triangular Pareto front
R2	0.9680	0.9760
New R2	**0.9977**	**0.9990**
R2-2	0.9965	0.9945
R2-4	0.9895	0.9969
R2-5	0.9779	0.9917

Table 5: MSE between hypervolume and R2 indicators in Section 4.3

Indicators	Triangular Pareto front	Inverted triangular Pareto front
R2	1.5539e-02	7.8506e-03
New R2	**4.2346e-04**	**4.7820e-05**
R2-2	2.1096e-03	1.7750e-03
R2-4	4.5866e-03	8.7147e-04
R2-5	1.2005e-02	3.3926e-03

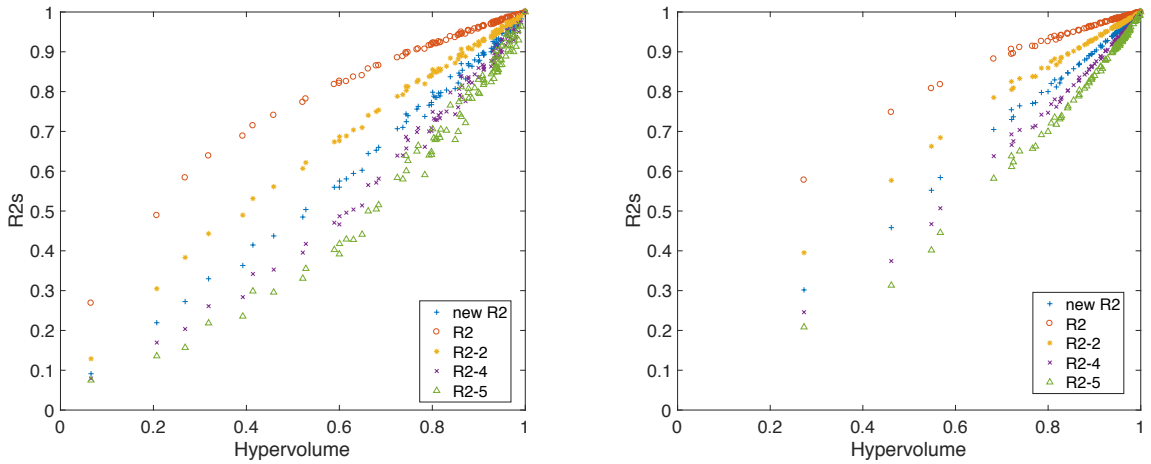

(a) Triangular Pareto front

(b) Inverted triangular Pareto front

Figure 11: Numerical results in Section 4.3.

5 CONCLUSIONS

In this paper, we proposed a new R2 indicator for better hypervolume approximation. Comprehensive numerical studies have demonstrated the superiority of the proposed new R2 indicator over several other R2 indicators for the hypervolume approximation. The new R2 indicator will bring new opportunities for the development of the indicator-based EMOAs. The current work is only the first step and more research will be conducted in the future. The R2 indicators are defined based on a set of direction vectors, and in current work we use the simplex lattice design method to generate the direction vectors. It will be interesting to test the approximation performance of the R2 indicators based on a different direction vector generation method [11, 12, 15]. Another future research direction is to develop the new R2 indicator-based EMOA and compare with the hypervolume-based EMOAs [2, 3] and other R2 indicator-based EMOAs [5, 6, 14, 16].

ACKNOWLEDGMENTS

This work was supported by the Science and Technology Innovation Committee Foundation of Shenzhen (Grant No. ZDSYS201703031748 284).

REFERENCES

[1] Johannes Bader, Kalyanmoy Deb, and Eckart Zitzler. 2010. Faster hypervolume-based search using Monte Carlo sampling. In *Multiple Criteria Decision Making for Sustainable Energy and Transportation Systems*. Springer, 313–326.

[2] Johannes Bader and Eckart Zitzler. 2011. HypE: An algorithm for fast hypervolume-based many-objective optimization. *Evolutionary computation* 19, 1 (2011), 45–76.

[3] Nicola Beume, Boris Naujoks, and Michael Emmerich. 2007. SMS-EMOA: Multiobjective selection based on dominated hypervolume. *European Journal of Operational Research* 181, 3 (2007), 1653–1669.

[4] Dimo Brockhoff, Tobias Wagner, and Heike Trautmann. 2012. On the properties of the R2 indicator. In *Proceedings of the 14th annual conference on Genetic and evolutionary computation*. ACM, 465–472.

[5] Dimo Brockhoff, Tobias Wagner, and Heike Trautmann. 2015. R2 indicator-based multiobjective search. *Evolutionary Computation* 23, 3 (2015), 369–395.

[6] Raquel Hernández Gómez and Carlos A Coello Coello. 2013. MOMBI: A new metaheuristic for many-objective optimization based on the R2 indicator. In *Evolutionary Computation (CEC), 2013 IEEE Congress on*. IEEE, 2488–2495.

[7] Michael Pilegaard Hansen and Andrzej Jaszkiewicz. 1998. *Evaluating the quality of approximations to the non-dominated set*. IMM, Department of Mathematical Modelling, Technical Universityof Denmark.

[8] Hisao Ishibuchi, Noritaka Tsukamoto, Yuji Sakane, and Yusuke Nojima. 2009. Hypervolume approximation using achievement scalarizing functions for evolutionary many-objective optimization. In *Evolutionary Computation, 2009. CEC'09. IEEE Congress on*. IEEE, 530–537.

[9] Hisao Ishibuchi, Noritaka Tsukamoto, Yuji Sakane, and Yusuke Nojima. 2010. Indicator-based evolutionary algorithm with hypervolume approximation by achievement scalarizing functions. In *Proceedings of the 12th annual conference on Genetic and evolutionary computation*. ACM, 527–534.

[10] Uwe Jaekel. 2011. A Monte Carlo method for high-dimensional volume estimation and application to polytopes. *Procedia Computer Science* 4 (2011), 1403–1411.

[11] Ke Li, Kalyanmoy Deb, Qingfu Zhang, and Sam Kwong. 2015. An evolutionary many-objective optimization algorithm based on dominance and decomposition. *IEEE Transactions on Evolutionary Computation* 19, 5 (2015), 694–716.

[12] Xiaoliang Ma, Yutao Qi, Lingling Li, Fang Liu, Licheng Jiao, and Jianshe Wu. 2014. MOEA/D with uniform decomposition measurement for many-objective problems. *Soft Computing* 18, 12 (2014), 2541–2564.

[13] Xiaoliang Ma, Qingfu Zhang, Junshan Yang, and Zexuan Zhu. 2017. On Tchebycheff Decomposition Approaches for Multi-objective Evolutionary Optimization. *IEEE Transactions on Evolutionary Computation* (2017).

[14] Dũng H Phan and Junichi Suzuki. 2013. R2-IBEA: R2 indicator based evolutionary algorithm for multiobjective optimization. In *Evolutionary Computation (CEC), 2013 IEEE Congress on*. IEEE, 1836–1845.

[15] Yan-Yan Tan, Yong-Chang Jiao, Hong Li, and Xin-Kuan Wang. 2013. MOEA/D+ uniform design: A new version of MOEA/D for optimization problems with many objectives. *Computers & Operations Research* 40, 6 (2013), 1648–1660.

[16] Heike Trautmann, Tobias Wagner, and Dimo Brockhoff. 2013. R2-EMOA: Focused multiobjective search using R2-indicator-based selection. In *International Conference on Learning and Intelligent Optimization*. Springer, 70–74.

[17] Tobias Wagner, Heike Trautmann, and Dimo Brockhoff. 2013. Preference articulation by means of the R2 indicator. In *International Conference on Evolutionary Multi-Criterion Optimization*. Springer, 81–95.

[18] Qingfu Zhang and Hui Li. 2007. MOEA/D: A multiobjective evolutionary algorithm based on decomposition. *IEEE Transactions on evolutionary computation* 11, 6 (2007), 712–731.

[19] Eckart Zitzler, Joshua Knowles, and Lothar Thiele. 2008. Quality assessment of pareto set approximations. *Multiobjective Optimization* (2008), 373–404.

[20] Eckart Zitzler and Lothar Thiele. 1998. Multiobjective optimization using evolutionary algorithms - a comparative case study. In *international conference on parallel problem solving from nature*. Springer, 292–301.